Electronic Supplementary Information

Stretchable Negative Poisson's Ratio Yarn for Triboelectric Nanogenerator as Environmental Energy Harvesting and Self-powered sensors

Lijun Chen,[a,b‡] Chaoyu Chen,[a,b‡] Long jin,[a‡] Hengyu Guo,[a,d] Aurelia Chi Wang,[a] Fanggang Ning,[e] Qiaoli Xu,[a,b] Zhaoqun Du,[b*] Fumei Wang,[b*] Zhong Lin Wang[a,c*]

[a] *School of Material Science and Engineering,Georgia Institute of Technology, Atlanta, GA 30332, United States. Email: zhong.wang@mse.gatech.edu*

[b] *Key Laboratory of Textile Science & Technology, Ministry of Education, College of Textiles, Donghua University, Shanghai 201620, P. R. China. Email: wfumei@dhu.edu.cn, duzq@dhu.edu.cn*

[c] *Beijing Institute of Nanoenergy and Nanosystems, Chinese Academy of Sciences Beijing 100083, P. R. China*

[d] *Department of Applied Physics, State Key Laboratory of Power Transmission Equipment & System Security and New Technology, Chongqing University, Chongqing, 400044 P. R. China*

[e] *Industrial Research Institute of Nonwovens and Technical Textiles, College of Textiles and Clothing, Qingdao University, Shandong, 266075, P. R. China*

† Electronic supplementary information (ESI) available in the online version, at…

‡ These authors contributed equally to this work.

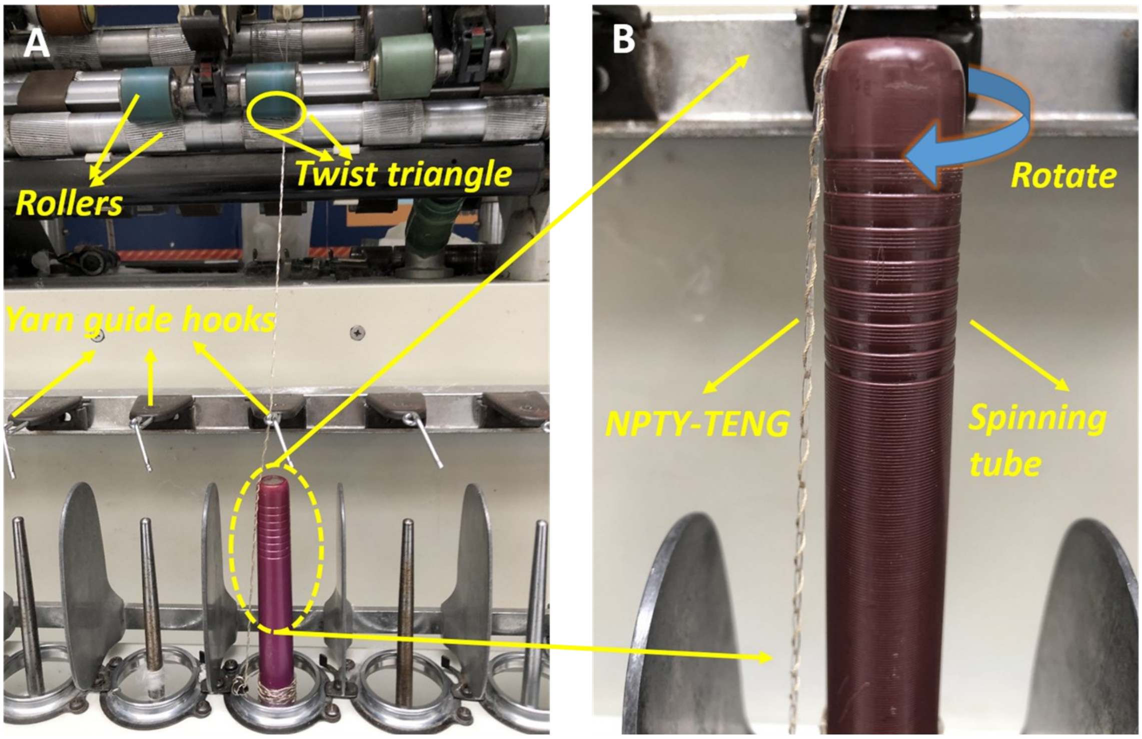

Fig. S1. The physical photographs of spinning frame. (A) The main part of the spinning frame. (B) The enlarged view of spinning tube.

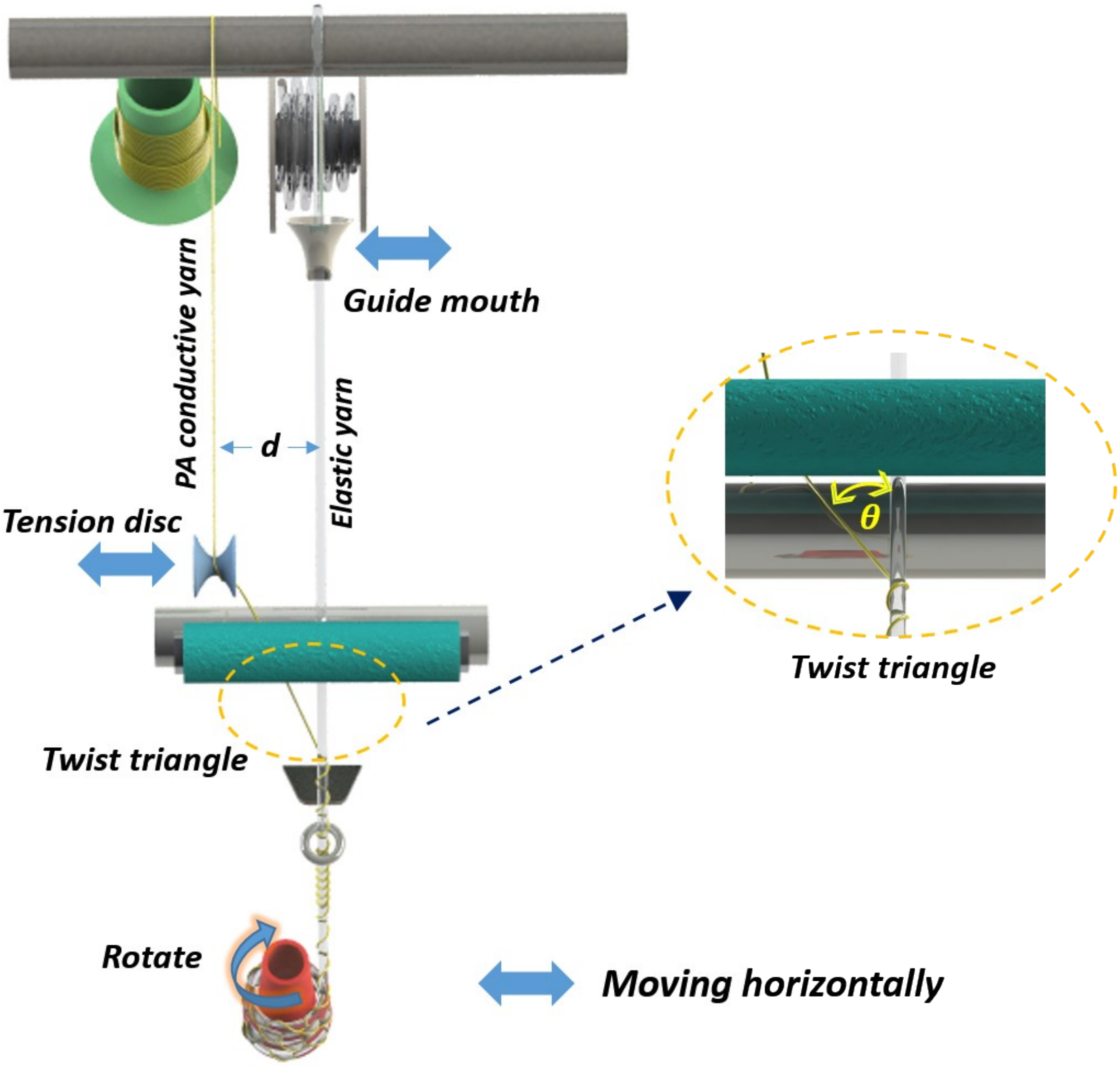

Fig. S2. The schematic illustration of the top view of the spinning frame.

Note S1: Cost estimate

Table S1 The price of raw materials

Item	Price
PA conductive yarn	$35/100 meter
TPU yarn (diameter 1.2mm)	$5/100 meter
TPU yarn (diameter 1.0mm)	$4/100 meter
TPU yarn (diameter 0.8mm)	$2.5/100 meter

For 1 meter of NPRY with TPU yarn (the maximum diameter 1.2mm) and (the minimum helix pitch h=3.75), the PA conductive yarn and TPU yarn we need will not exceed 1.2 meters. So the raw material cost for 1 meter of NPRY will less than $0.48.

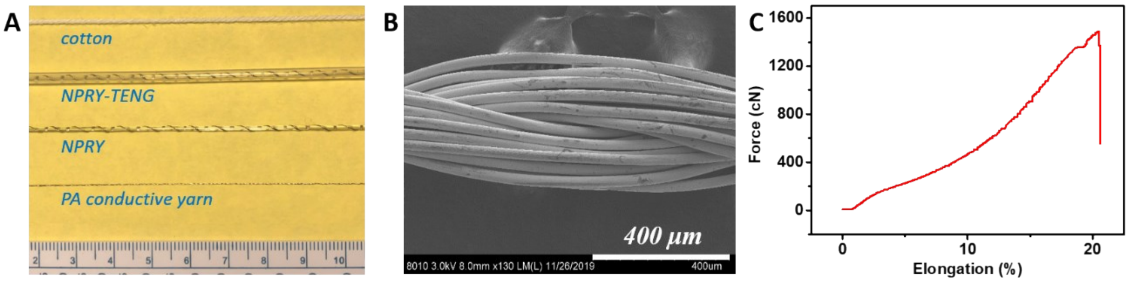

Fig. S3. The physical photograph, scanning electron microscope (SEM) image and tensile property of PA conductive yarn.(A) The Physical photograph of PA conductive yarn, NPRY, NPRY-TENG and cotton yarn. (B) The SEM image of two-ply twisted PA conductive yarn. (C) The tensile property of PA conductive yarn.

Note S2: The calculation of Poisson's ratio

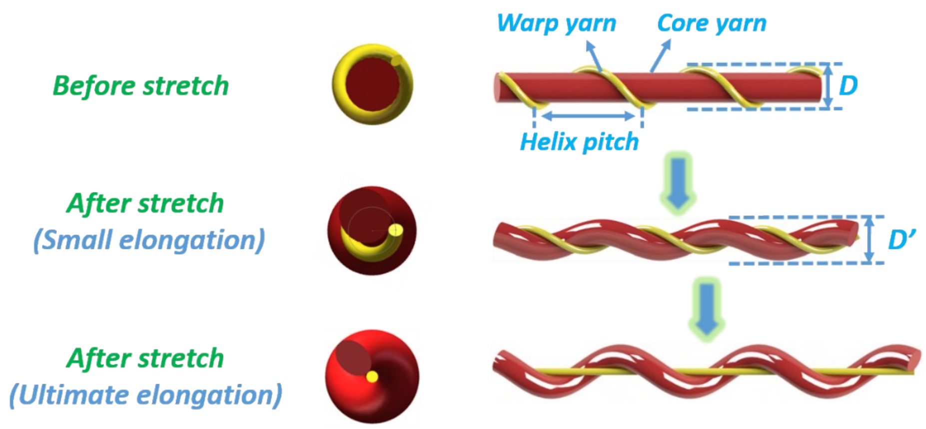

Fig. S4. The schematic illustration of changes of the yarn shape when NPRY is stretched.

$$\varepsilon_t = \frac{D^{'} - D}{D} \tag{1}$$

$$\sigma = -\frac{\varepsilon_t}{\varepsilon_l} \tag{2}$$

As shown in Fig. S4, D is the original diameter of NPRY and $D^{'}$ is the diameter of the NPRY after stretch. So the transverse strain ε_t can be calculated by Equation (1). And the Poisson's ratio σ can be calculated by Equation (2). Where, ε_l is the Longitudinal elongation.

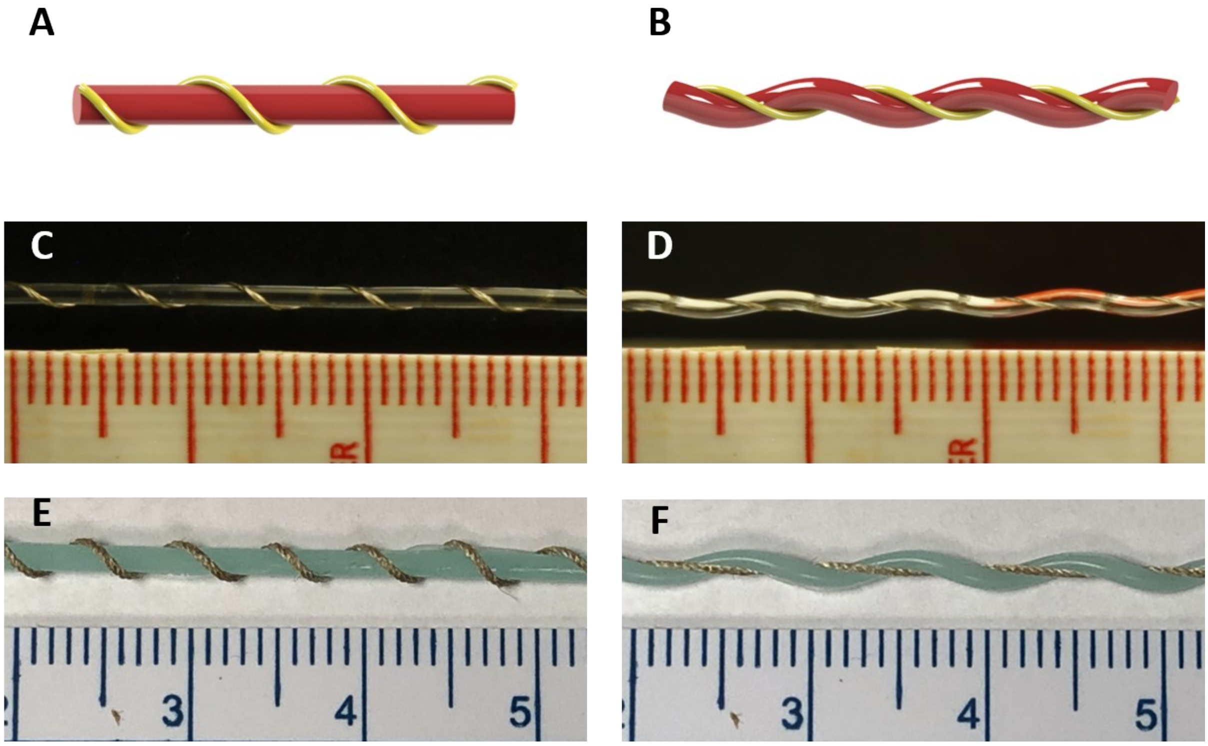

Fig. S5. The schematic illustration and Physical photographs of different NPRYs before and after stretch. (A and B) The schematic illustration NPRYs before and after stretch. (C and D) The Physical photographs of NPTY consisted of two-ply twisted PA conductive yarn and TPU yarn. (E and F) The Physical photographs of NPTY consisted of four-ply twisted PA conductive yarn and silicone rubber yarn.

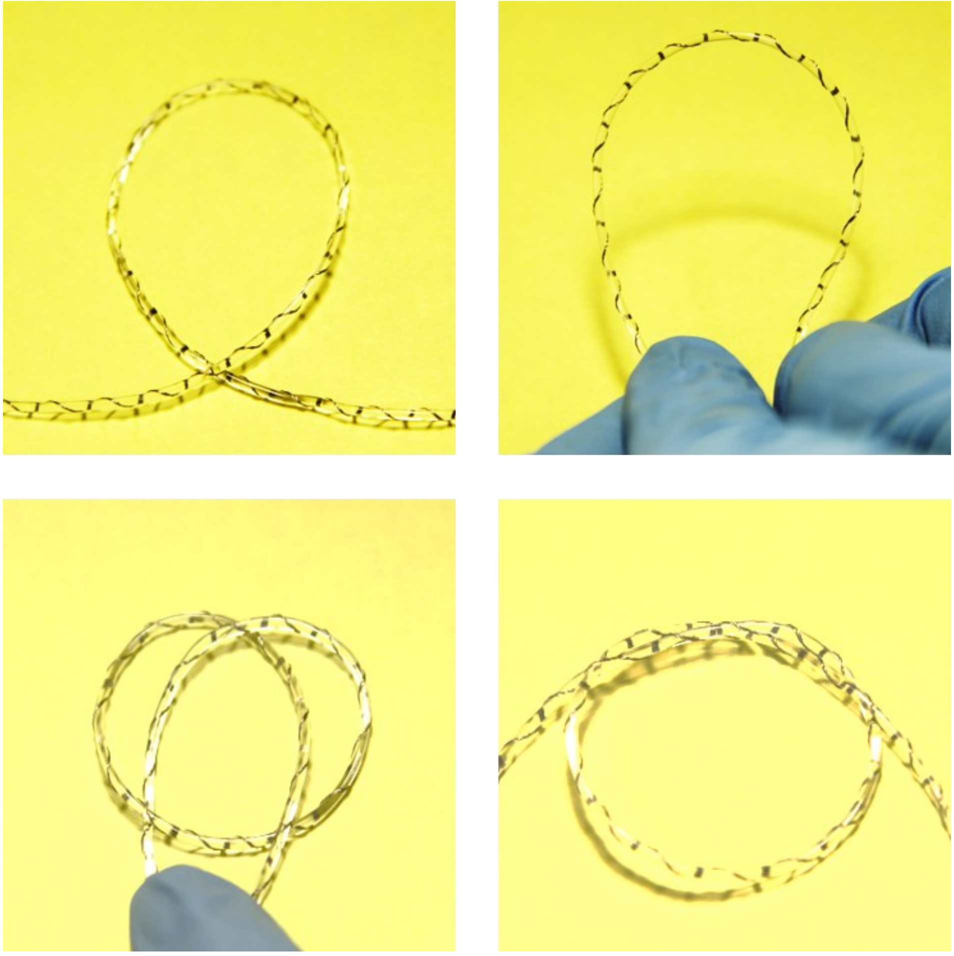

Fig. S6. The photographs of NPRY under arbitrary complex deformations.

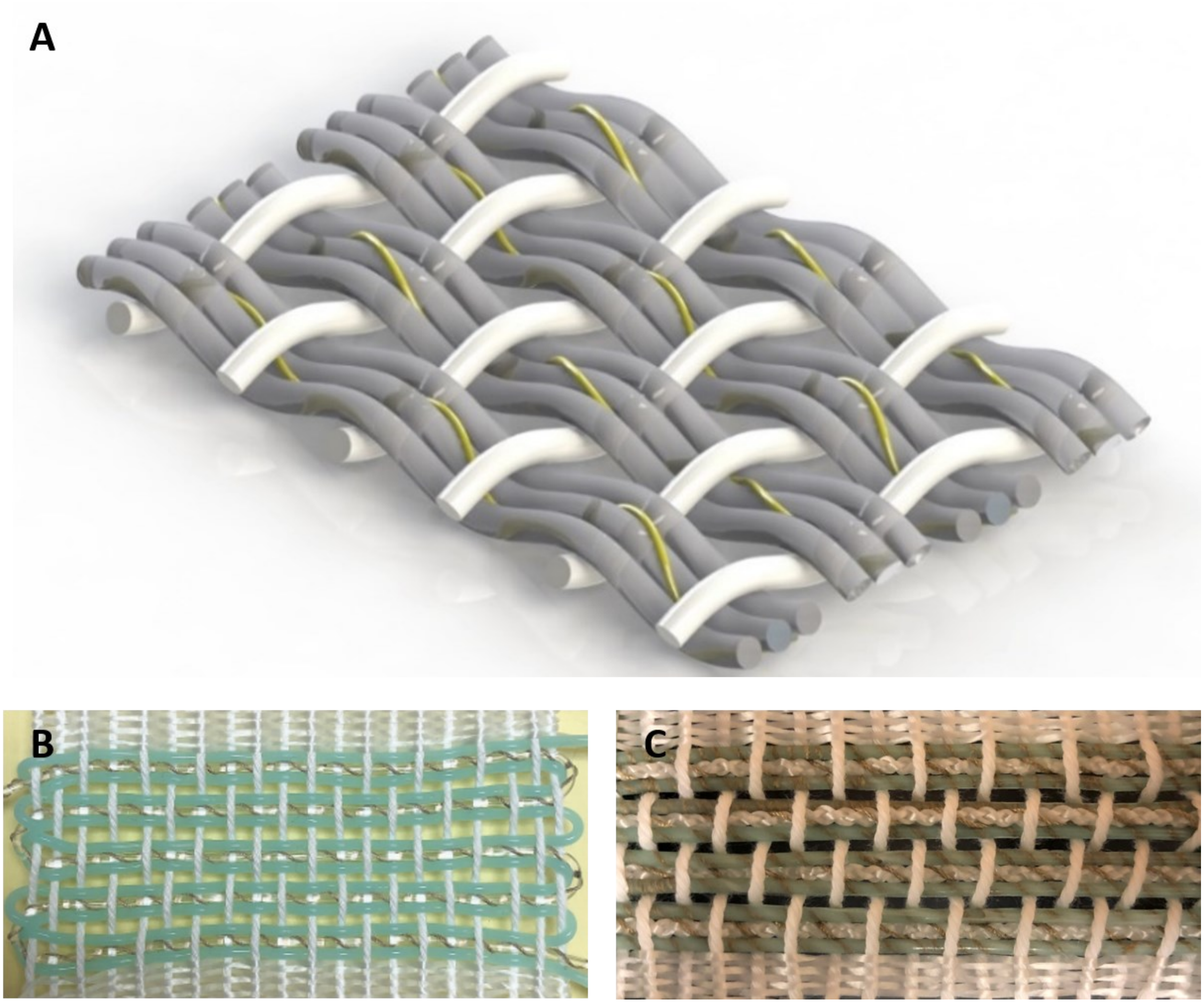

Fig. S7. The schematic illustration and physical photographs of NPRY fabric TENG. (A) The schematic illustration of NPRY fabric TENG from isometric view. (B and C) The physical photographs of NPRY fabric TENG manufactured by different NPRYs.

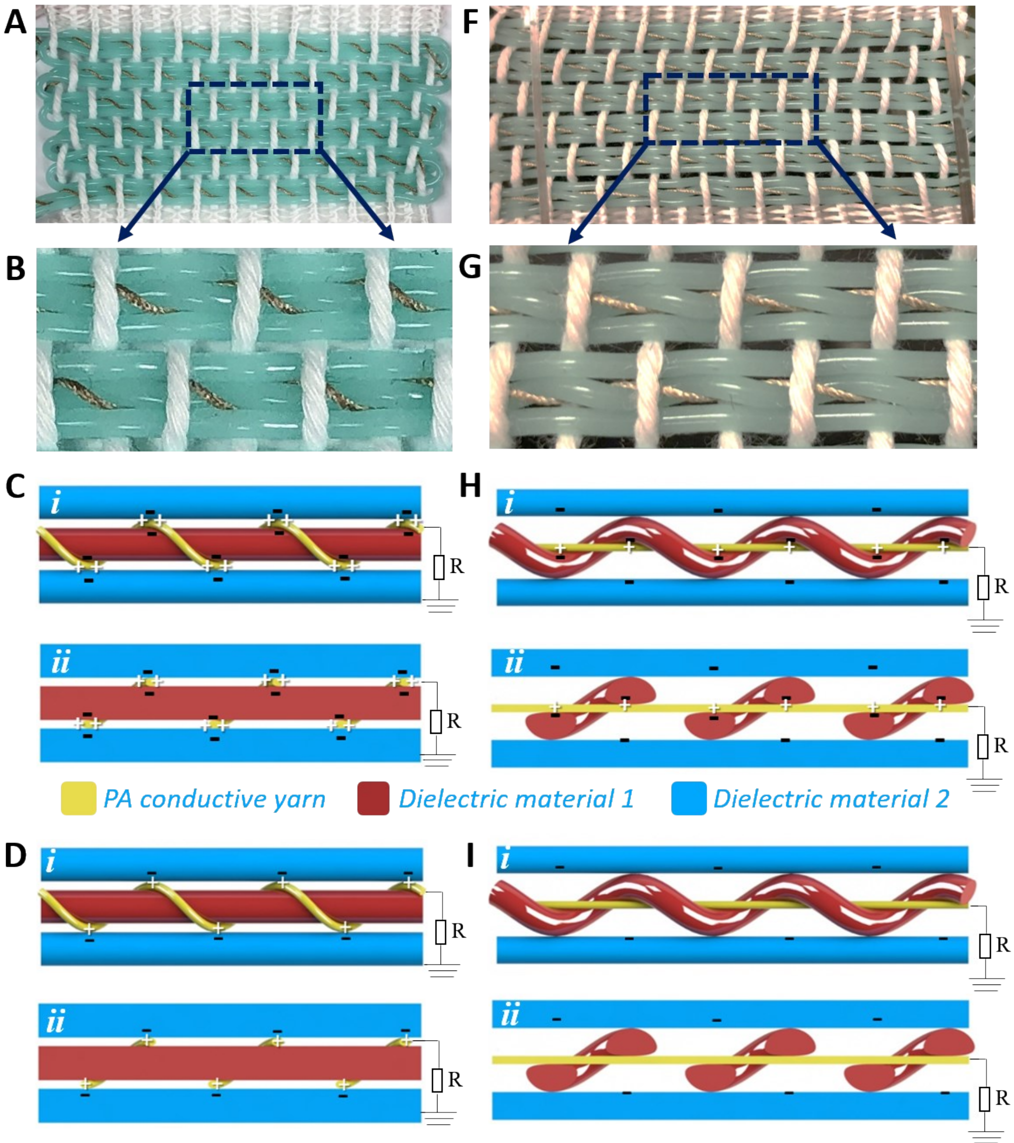

Fig. S8. The physical photographs and working mechanism of NPRY fabric TENG. (A and B)The physical photographs of NPRY fabric TENG before stretch. (C and D)The charge distribution on NPRY fabric TENG before stretch. (F and G) The physical photographs of NPRY fabric TENG after stretch. (H and I) The charge distribution on NPRY fabric TENG after stretch.

Note S3: The working mechanism for NPRY fabric TENG

The working mechanism for NPRY fabric TENG are shown in Fig. S8C and S8H. And Fig. S8C(ii) and S8H(ii) are the cross section of Fig. S8C(i) and S8H(i). We assume that dielectric material 1 and dielectric material 2 can both obtain negative charges from PA conductive yarn when they contact with each other as shown in Fig. S8C. After stretch, as shown in Fig. S8F, PA conductive yarn will be the core yarn and dielectric material 1 will be the warping yarn. During the stretching process, PA conductive yarn and dielectric material 2 will separate from each other. The attraction of the negative charges on the surface of PA conductive yarn and the positive charges on the surface of dielectric material 2 will decrease or disappear. Due to electrostatic induction, the negative charges from earth will neutralize part of the positive charges on the surface of PA conductive yarn. However, PA conductive yarn and dielectric material 1 always contact with each other tightly. So after stretch, there will always be a constant amount of positive charge on the surface of PA conductive yarn attracted by negative charges on the surface of dielectric material 1. Comparing the charge distribution on NPRY fabric TENG before stretch (Fig.

S8C) and after stretch (Fig. S8H), we can draw a conclusion that no matter what dielectric material 1 is (easy to get electrons or lose electrons), it has no effect on the output performance of NPRY. Therefore, the charge distribution on NPRY fabric TENG can be simplified as shown in Fig. S8D and Fig. S8I.

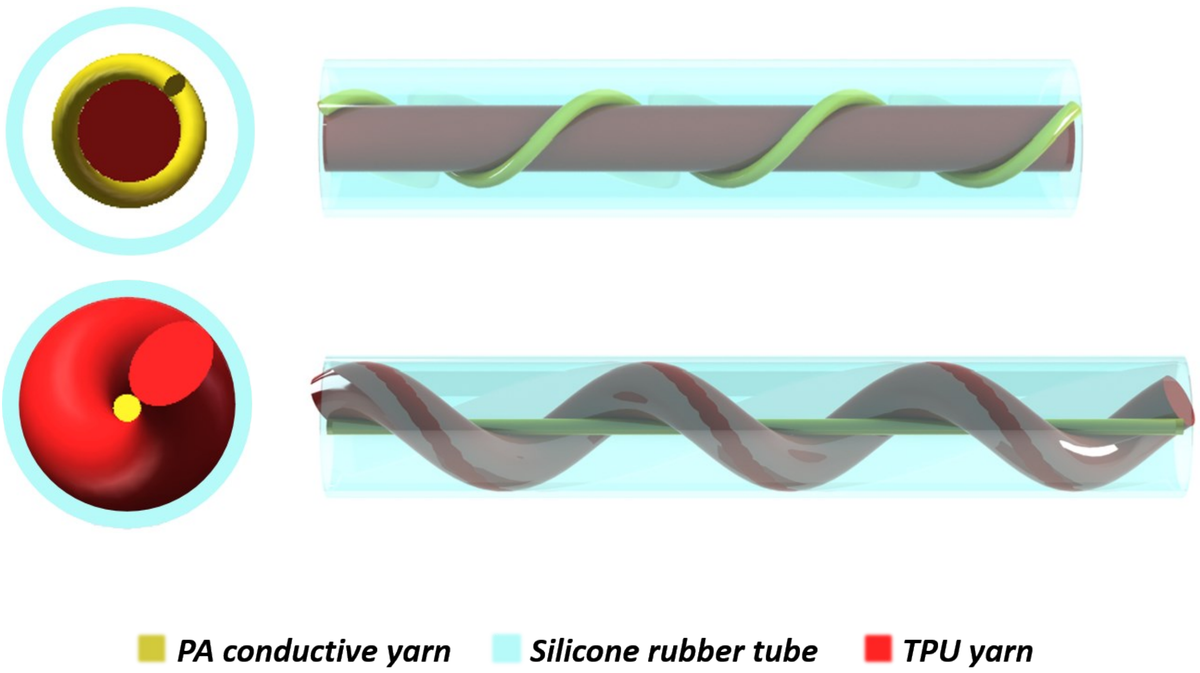

Fig. S9. The schematic illustration of cross sections and side views of NPRY-TENG before stretch and after stretch.

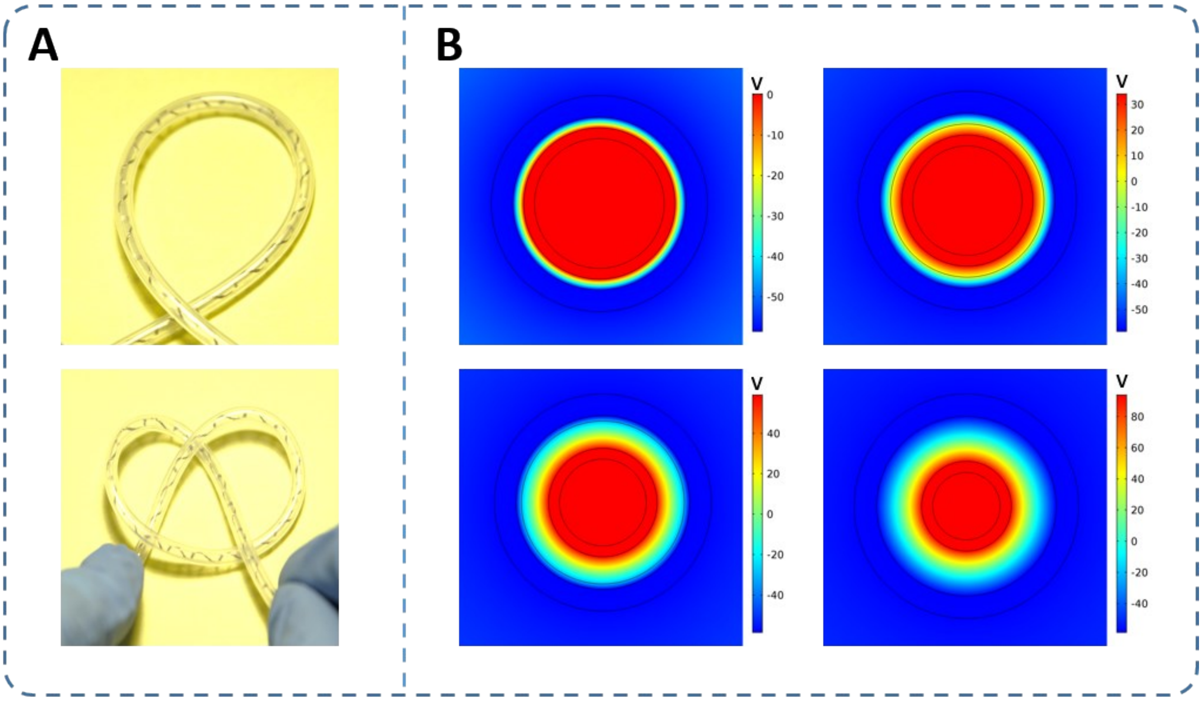

Fig. S10. The physical photographs and working mechanism of NPRY-TENG. (A) The photographs of NPRY under arbitrary complex deformations.(B) The working mechanism of NPRY-TENG.

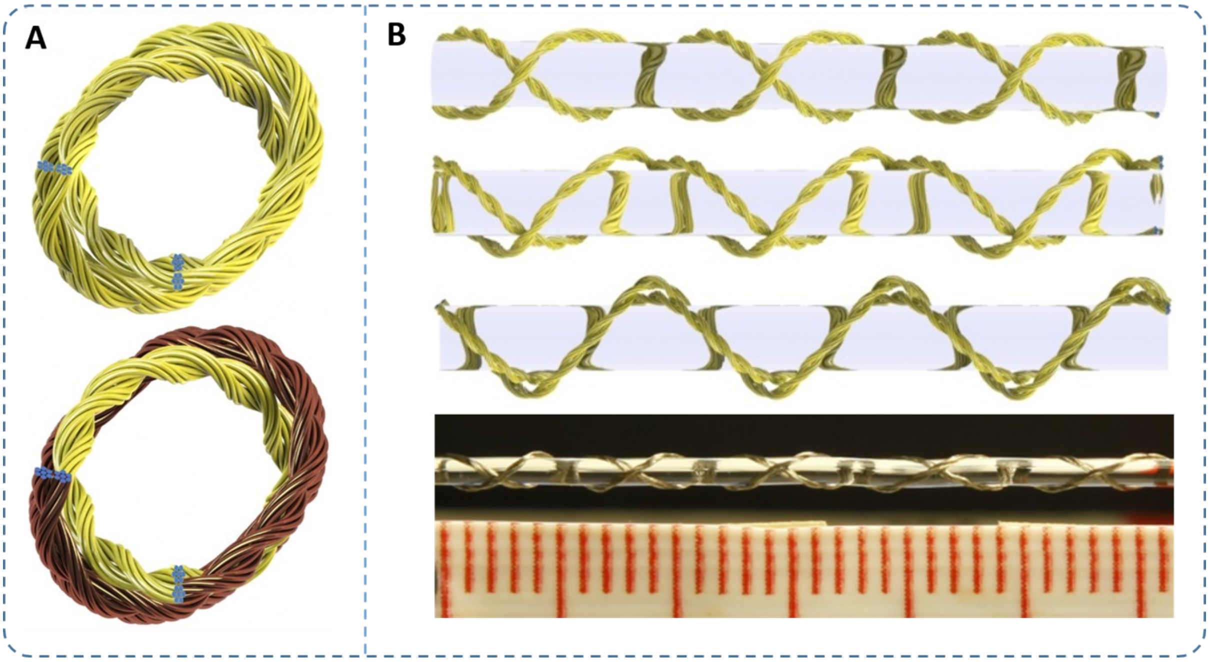

Fig. S11. The schematic illustration and physical photograph of Cross sections and side views of NPRY with interlocked helix structure. (A) The cross sections of NPRY with interlocked helix structure. (B) The schematic illustration and physical photograph of side views of NPRY with interlocked helix structure

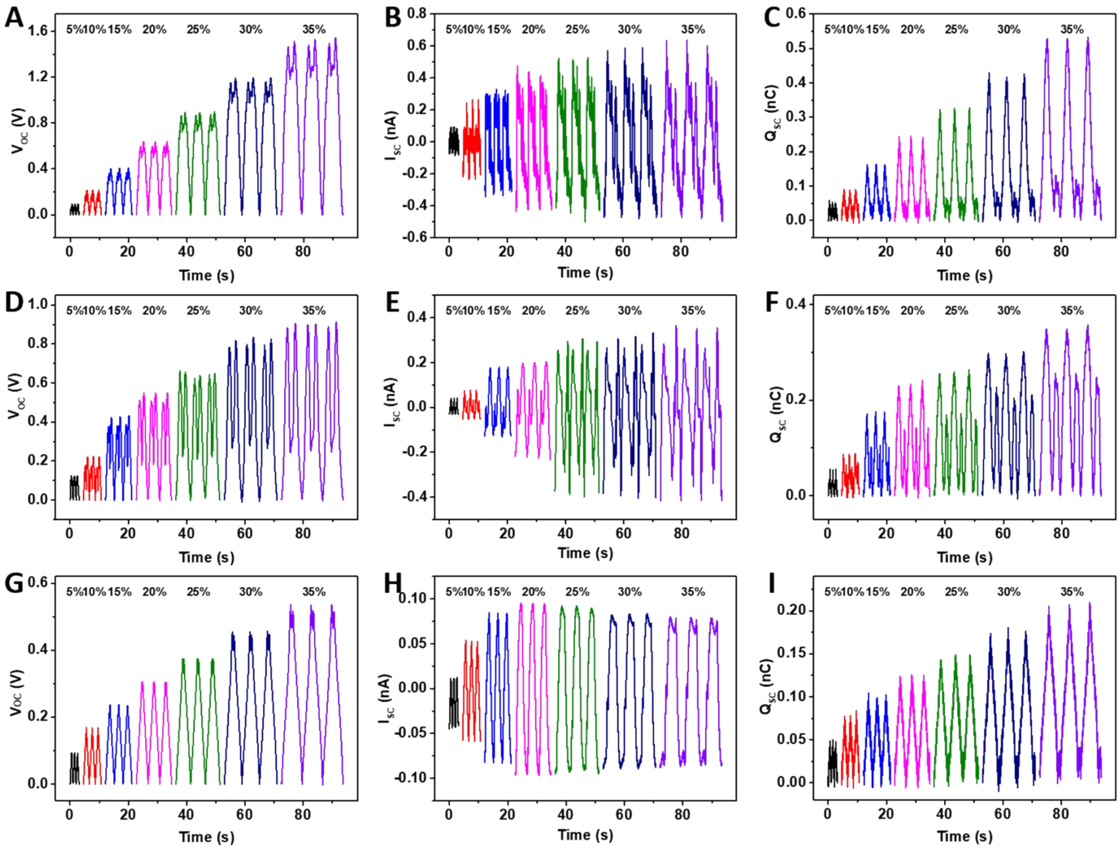

Fig. S12. The output performance of NPRY-TENG with different structure and different materials. (A to C) The output performance of NPRY-TENG with single helix structure and silicone rubber tube. (D to F) The output performance of NPRY-TENG with interlocked helix structure and silicone rubber tube. (G to I) The output performance of NPRY-TENG with single helix structure and Latex rubber tube.

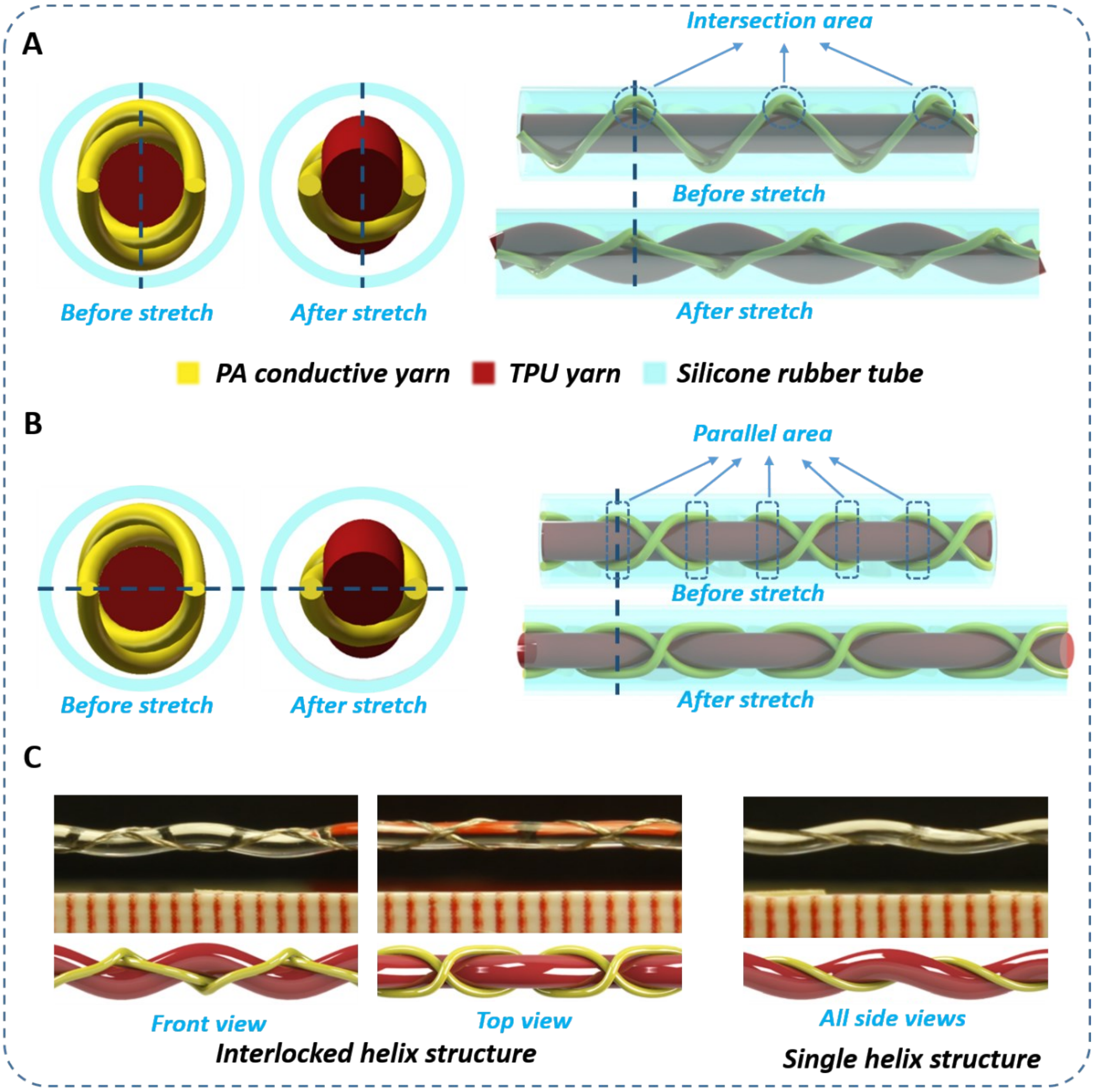

Fig. S13. The schematic illustration of cross sections and side views of interlocked helix structure NPRY-TENG before and after stretch. (A) The deformation of intersection point for PA conductive yarns before and after stretch. (B) The deformation of parallel point for PA conductive yarns before and after stretch. (C) The physical photographs and schematic illustration of NPRY with interlocked helix structure and single helix structure after stretch.

Note S4: Contact area analysis

As shown in Fig. S13, the TPU yarns and PA conductive yarns deform in different way after stretch. For NPRY-TENG with interlocked helix structure after stretch, the schematic illustration and physical photographs present a sine wave in front view, but a straight line in top view, which demonstrates that interlocked helix structure restricts the deformation of NPRY in one direction, and the TPU yarn and two conductive yarns can only deform like a sine wave. Therefore, as shown in Fig. S13a,b, only the intersection area can be effective contact area between PA conductive yarn and silicone rubber tube. While, for NPRY-TENG with single helix structure after stretch, the physical photograph present a sine wave in all side views, which demonstrates that the TPU yarn and the one PA conductive yarn can deform as a standard cylindrical spiral line (not ellipse or other shapes). So the entire PA conductive yarn can contact and separate with silicone rubber effectively.

Compared with the whole PA conductive yarn, the intersection area is smaller. So the output performance of NPRY-TENG with single helix structure is better than that of NPRY-TENG with interlocked helix structure

Note S5: Theoretical calculation

As shown in Figure 4a, r is the distance of "OA" in the cross section of NPRY. Here, "O" is the center of the cross section of NPRY and "A" is the center of PA conductive yarn. r_0 is the original value of r before stretch. So D_0 can be express as follow:

$$D_0 = 2r_0 = 2(r_{TPU} + r_{PA}) \tag{3}$$

Where, r_{TPU} and r_{PA} is the radius of TPU yarn and PA conductive yarn, respectively.

h is the helix pitch (Fig. S4) of NPRY. l is the length of PA conductive yarn. When the PA conductive yarn spreads along the cylinder (TPU yarn). πD_0, l, and h can from a right triangle. Their relationship can be express as Equation (3):

$$l = \sqrt{h^2 + \pi^2 D_0^2} \tag{4}$$

When the elongation is ε after stretch, the helix pitch is $h(1+\varepsilon)$. Compared with the elastic modulus TPU yarn, the elastic modulus of PA conductive yarn is very high. We assume that PA conductive yarn is rigid body. That is, the length "l" of PA conductive yarn won't change. So we can get the Equation (4):

$$l = \sqrt{h^2(1+\varepsilon)^2 + \pi^2 D_\varepsilon^2} \tag{5}$$

Where, $D_\varepsilon = 2r_\varepsilon$. Combine with Equation (4) and Equation (5), D_ε can be express as follow:

$$D_\varepsilon = \sqrt{D_0 - \frac{h^2}{\pi^2}(\varepsilon^2 + 2\varepsilon)} \tag{6}$$

So we can calculated the variation "Δr" of r when elongation ε increases by Equation as follow:

$$\Delta r = r_0 - r_\varepsilon = \frac{D_0 - D_\varepsilon}{2} \tag{7}$$

Combine with Equation (6) and Equation (3), Δr can be express as follow:

$$\Delta r = r_{TPU} + r_{PA} - \frac{1}{2}\sqrt{2r_{TPU} + 2r_{PA} - \frac{h^2}{\pi^2}(\varepsilon^2 + 2\varepsilon)} \tag{8}$$

If $D_\varepsilon = 0$, Δr and ε will get the maximum value:

$$\Delta r_{max} = r_{TPU} + r_{PA} \tag{9}$$

$$\varepsilon_{max} = \frac{\sqrt{\pi^2 D_0^2 + h^2}}{h} - 1 \tag{10}$$

Note 6: The contrastive analysis between the data of Fig. 4B, 4C and Fig. 4D-G

In Fig. 4B, when the elongation and the helix pitch (h=6.25 mm) is the same, Δr (Note S5) of NPRY with minimum diameter (DTPU=0.8 mm) is the biggest. That is, for NPRY-TENG with a smaller DTPU, the PA conductive yarn will be farther away from the tube when the elongation and the helix pitch h is the same. For experimental result in Fig. 4D and 4E, when elongation is same and smaller than 25%, the VOC and QSC of NPRY with minimum diameter (DTPU=0.8 mm) is the biggest; the VOC and QSC of NPRY with minimum diameter (DTPU=1.0 mm) is in the middle; the VOC and QSC of NPRY with minimum diameter (DTPU=0.8 mm) is the smallest. The experimental data is exactly the same as theoretical calculation. It is same situation with the data in Fig. 4C and Fig. 4F, 4G. So, the theoretical calculation match to the output performance very well when elongation is lower than 25%-30%.

The shortcoming of theoretical analysis is that theoretical calcaulation and experimental data are mismatched when the elongation is larger than 25%-30%. Two reasons are thought to be responsible for the shortcoming. The first one, the breaking elongation of PA conductive yarn is about 20% as shown in Fig. S3C. So the biggest elongation of some NPRYs with different structure parameters in Fig. 4D-4G are larger than the biggest elongation in Figure 4B, 4C. The second one, according to the theoretical analysis (Note S5, ESI†), Δr will reach the maximum Δr_{max}($\Delta r_{max} = r_{TPU} + r_{PA}$) which is a constant value when $D_{\varepsilon} = 0$. However, in reality, the diameter (or radius, r_{TPU} and r_{PA}) of PA conductive yarn and TPU yarn will decrease when the PA conductive yarn is basically straight and continues to be stretched. So Δr will increases to the biggest slowly and then decreases. As a result, in reality, with the increase of the elongation, the distance between PA conductive yarn and silicone rubber tube will first increase to the maximum and then decrease. Therefore the VOC and QSC of NPRY-TENG will first increase to the maximum and then decrease with the elongation increasing.

Taking these two reasons into account, the theoretical analysis is relatively accurate for all elongation.

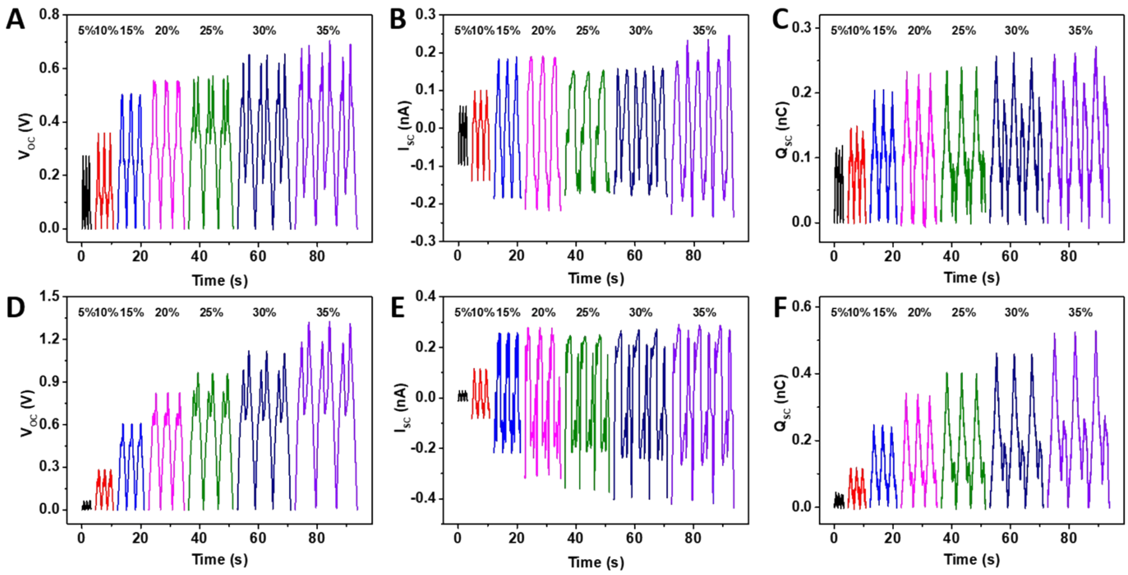

Fig. S14. The output performance of NPRY-TENG with TPU yarns of different diameters. (A to C) The output performance of NPRY-TENG with TPU yarns (diameter is 0.8mm). (D to F) The output performance of NPRY-TENG with TPU yarns (diameter is 1.0 mm)

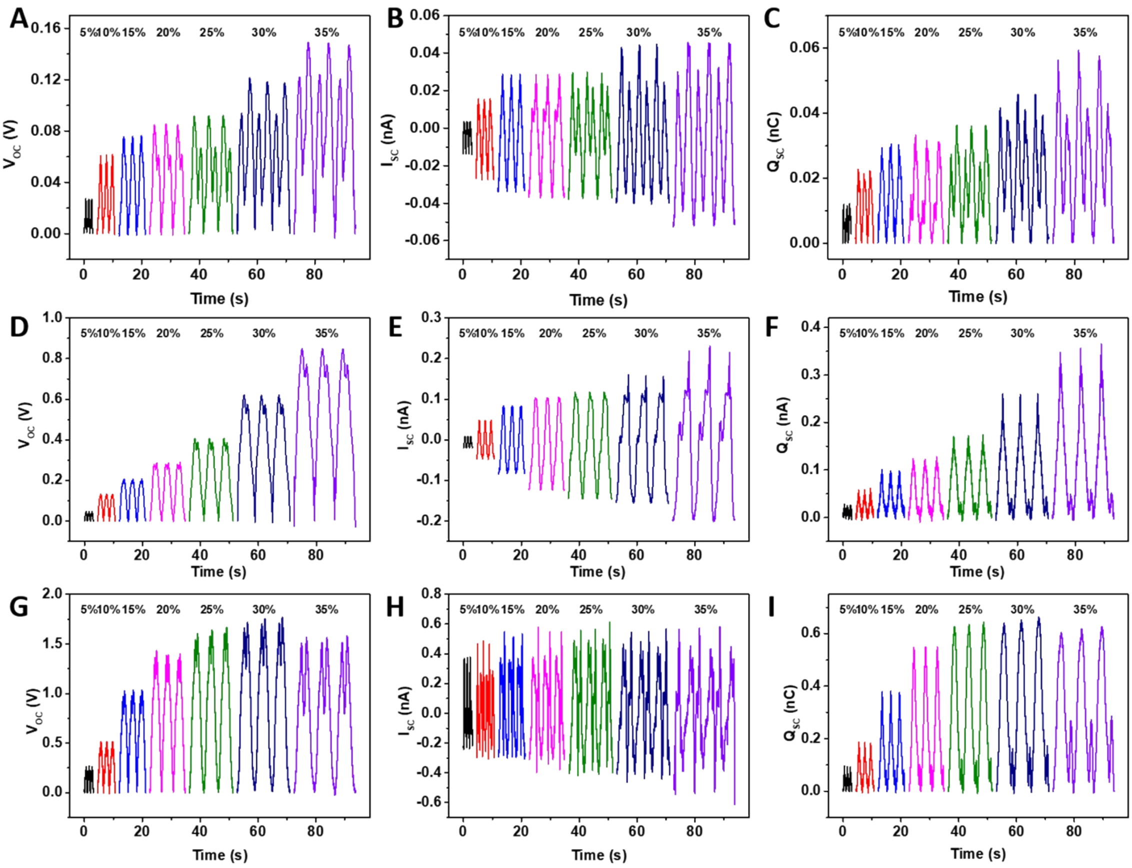

Fig. S15. The output performance of NPRY-TENG with different helix pitches. (A to C) The output performance of NPRY-TENG with helix pitch of 3.75 mm. (D to F) The output performance of NPRY-TENG with helix pitch of 5 mm. (G to I) The output performance of NPRY-TENG with helix pitch of 7.5 mm.

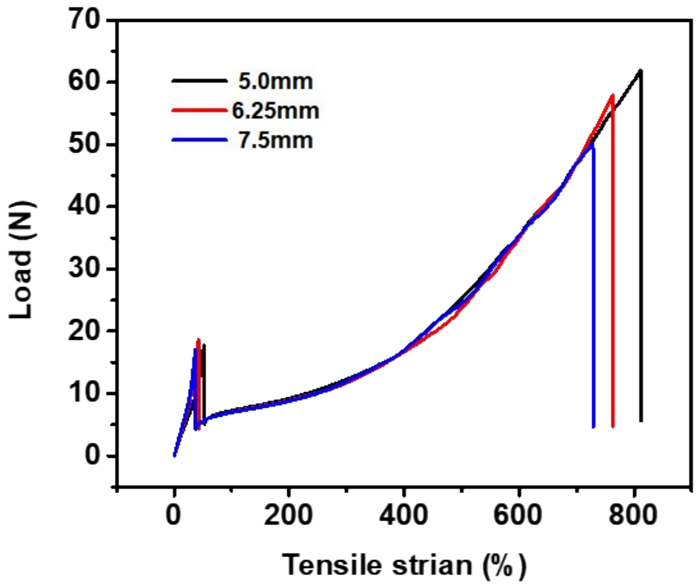

Fig. S16. The stress–strain curves of NPRY with different helix pitches

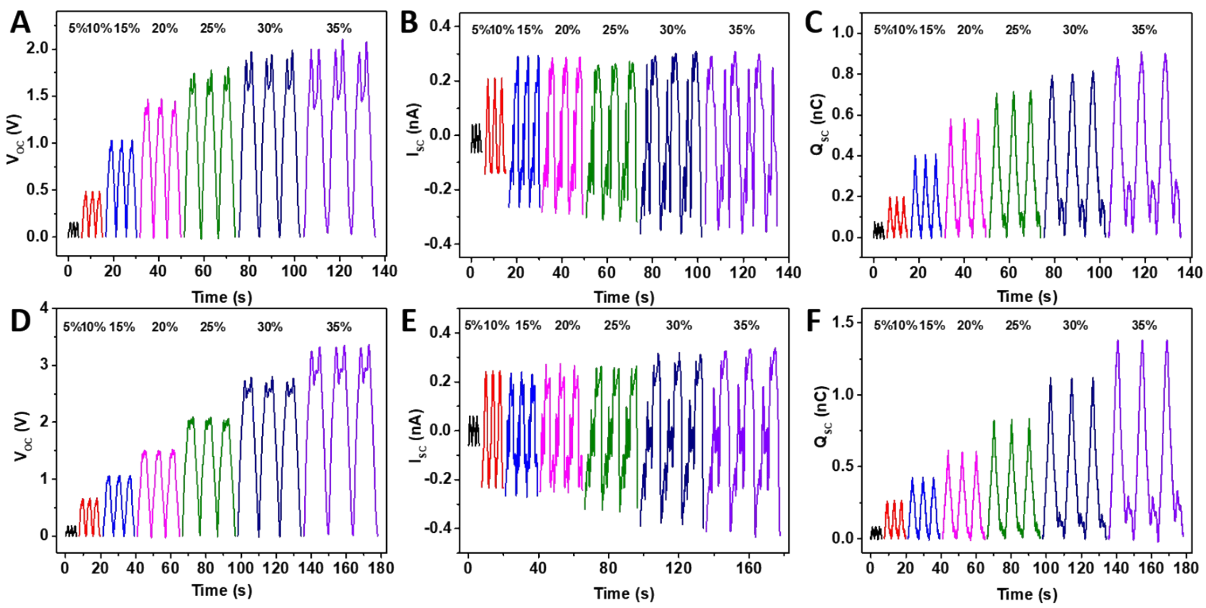

Fig. S17. The output performance of NPRY-TENG with different lengths. (A to C) The output performance of NPRY-TENG with length of 15 cm. (D to F) The output performance of NPRY-TENG with length of 20 cm.

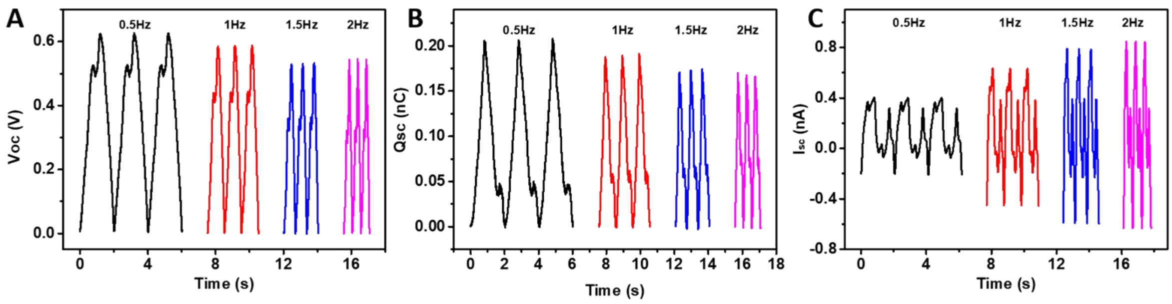

Fig. S18. The electrical output performances of the NPRY-TENG stretched at a certain elongation (15%) under different frequencies (0.5-2 Hz). (A) V_{OC}, (B)I_{SC}, (C) $Q_{SC.}$

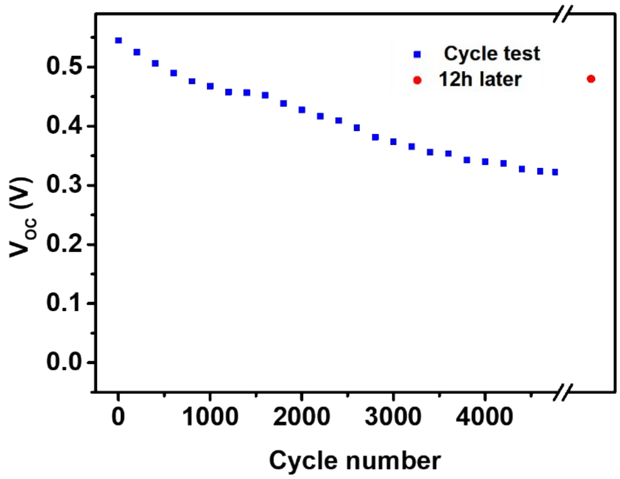

Fig. S19 The stability test of a NPRY-TENG.

Movie S1：The spinning process of NPRY on spinning frame.

Movie S2：Demonstration of the NPRY-TENG as a self-counting yoga elastic band.

Movie S3：Demonstration of the NPRY-TENG as an early warning self-powered sensor.

Movie S4：Demonstration of lighting LEDs letters by NPRY-TENG fabric.